



Supplement of

Present and future thermal regimes of intertidal groundwater springs in a threatened coastal ecosystem

Jason J. KarisAllen et al.

Correspondence to: Barret L. Kurylyk (barret.kurylyk@dal.ca)

The copyright of individual parts of the supplement might differ from the article licence.

Summary of image analysis (box 1, Figure 2 and Figure 5, main text): Rather than developing a per-pixel corrections matrix for the sensor to correct for distortion towards the image periphery, only the central portion of each image was analysed. This study applied FLIR Tools®, ImageJ, and MATLAB® to post-process grayscale intensity data from the thermal infrared images using the procedure summarized in Fig. S1. These products enabled the analysis of high-resolution thermal data and polygonal cropping procedures. Grayscale intensity data was extracted from the thermal images of the spring-sourced plumes and graphed with respect to cumulative area to yield a characteristic S-shape type-curve (Fig. S1). Each ‘inflection point’ of the graph was used to define ‘thermal groups’ and the sharp transition zones between them

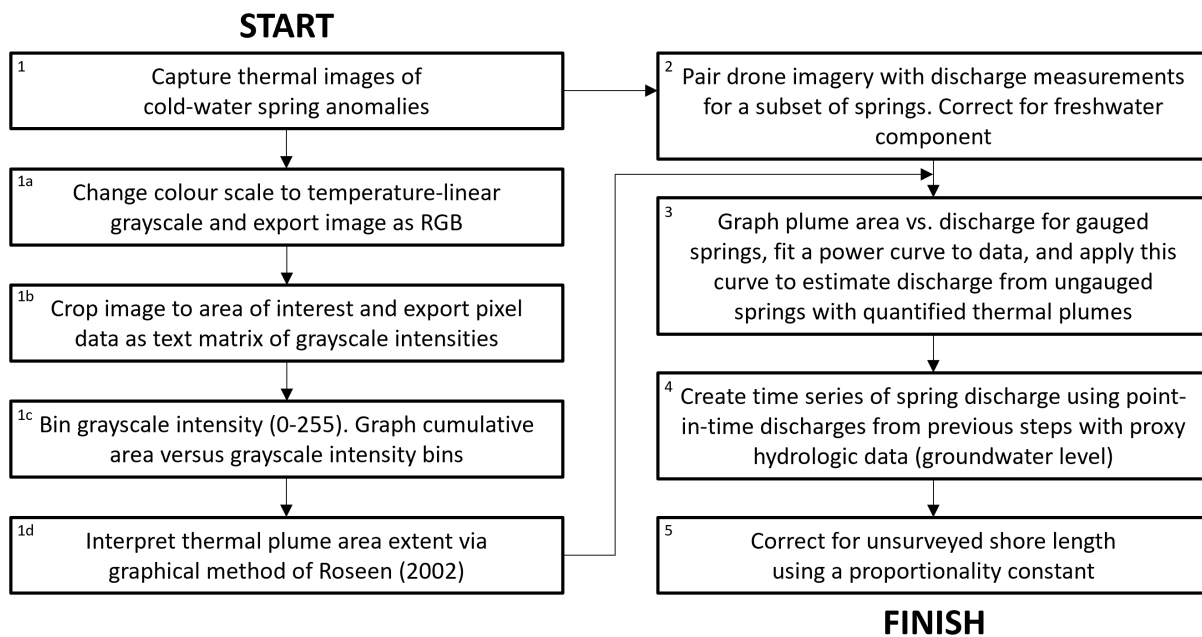


Figure S1: Summary workflow of the spring discharge assessment technique applied in Basin Head lagoon using thermal imagery. Panels a, b, c, and d of Fig. 5 correspond with box numbers 1, 1b, 1c, and 3, respectively

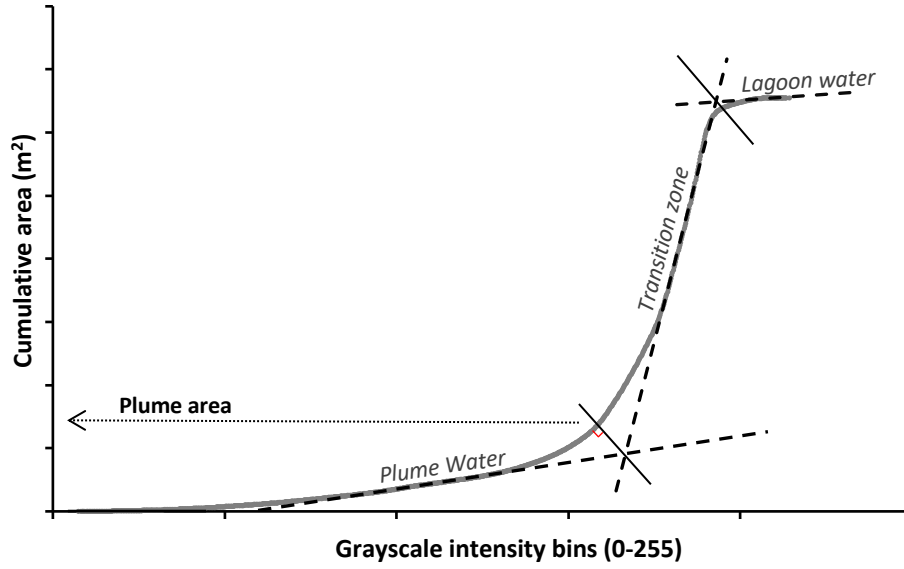


Figure S2. Generic characteristic type-curve used in the areal analysis of a thermal-discharge assessment (see step 1d of Fig. S1). Inflection points are identified using near-perpendicular lines connecting the type-curve and the linear intersects. The plume thermal group (i.e., plume area) extends to the plume area inflection point. The lagoon thermal group begins at the second inflection point and extends onward, and there is a steep transition zone between groups. See Roseen (2002) for a description of a similar approach.

Tables begin on the following page.

Table S1: Information on sensors deployed for this study. See figures in the Figure Reference column for locations. The IDs in the Map ID column in this table align with the IDs noted in Fig. S3-S6 in this supplement. All associated data can be found in the dataset described in the Data Availability section at the end of the main paper.

	Parameter(s) Provided	Sensor Make/Model	Number of Sensors	Map ID (prefix and ID#)	Approximate Location(s) by ID# (Long, Lat)	Data Period Provided (Discontinuous and varies per parameter)	Figure Reference(s)
Streams	Water temperature	Onset HOBO MX2203 TidbiTs	4	St1, 2, 3, and 4	1) 62.1243660°W 46.3865830°N 2) 62.1246730°W 46.3862840°N 3) 62.0914720°W 46.3957510°N 4) 62.0889510°W 46.3971560°N	Start: 2020-07-21 11:15 End: 2020-11-02 16:30	1 and 6
	Water flow	HOBOU20-001-04 & SonTek Flow Tracker 2	4	St5, 6, 7, and 8	5) 62.1273340°W 46.3867770°N 6) 62.1270000°W 46.3900000°N 7) 62.0952870°W 46.3974070°N 8) 62.0906230°W 46.3987880°N	Start: 2020-07-21 13:00 End: 2020-08-31 23:00	1 and S8
Springs	Water temperature	Onset HOBO MX2203 TidbiTs	2	Sp2 and 21	1) 62.1194598°W 46.3848724°N 2) 62.0998038°W 46.3905342°N	Start: 2020-07-25 17:30 End: 2020-11-02 16:30	1, 6, 7, S3, S4, and S5
	Water temperature	Onset HOBO MX2203 TidbiTs	1	Sp5	3) 62.0889360°W 46.3941150°N	Start: 2019-06-26 0:00 End: 2020-11-02 16:30	1, 7, S3, S6, and S7
Lagoon	Water temperature	Onset HOBO MX2203 TidbiTs	2	L3 and 4	3&4) 62.0879200°W 46.3950140°N	Start: 2019-06-26 2:45 End: 2020-11-02 16:30	1, 6, and S7
	Water temperature	Onset HOBO MX2203 TidbiTs	2	L1 and 2	1&2) 62.0953385°W 46.3910513°N	Start: 2020-07-25 15:30 End: 2020-11-02 16:30	1 and S7
	Water temperature and pressure	Solinst Levellogger 5 LTC	1	L5	5) 62.1106386°W 46.3817063°N	Start: 2020-07-21 12:30 End: 2020-11-02 16:30	1, 6, and S7
Piezometer	Water temperature and pressure	Onset HOBO U20-001-01	1	P1	1) 62.1020736°W 46.3900142°N	Start: 2019-08-17 14:45 End: 2020-11-02 16:30	1, S7
Climate Station	Air temperature, radiation, and precipitation	Onset HOBO Micro Station Logger	1	Cl1	1) 62.1030470°W 46.3890710°N	Start: 2019-06-26 0:00 End: 2020-11-02 16:30	1, 6, and S7

Table S2: Measured thermal plume areas of 34 springs in Basin Head lagoon over the study period (locations displayed in Figure 1b and Figures S3-S6). The instantaneous discharge of Springs A, B, and C (grey rows) were measured and used to develop the plume size-spring discharge relationship, whereas Springs 1-31 were estimated using their measured area and the developed relationship. The date/time indicates when the thermal image was captured. Areas were obtained as indicated in Figures S1 and S2 and included short distances of overland flow.

Spring ID	Date/time	Area (m ²)	Discharge (m ³ s ⁻¹)	Spring location (Lat; Long)
A	22-07-2020 19:37	360	3.1E-03*	46.389305; -62.102322
B	22-07-2020 19:35	51	5.2E-04*	46.390244; -62.10096
C	22-07-2020 19:36	10	7.5E-05*	46.388714; -62.103432
1	29-08-2020 15:27	694	6.2E-03	46.386246; -62.110306
2	29-08-2020 15:33	360	3.1E-03	46.38493; -62.119438
3	24-07-2020 19:33	289	2.5E-03	46.390179; -62.101189
4	22-07-2020 19:36	259	2.2E-03	46.396149; -62.08857
5	21-07-2020 20:17	171	1.4E-03	46.394167; -62.088889
6	24-07-2020 18:16	164	1.4E-03	46.386944; -62.115067
7	24-07-2020 18:16	133	1.1E-03	46.386944; -62.115067
8	24-07-2020 19:29	115	9.6E-04	46.39827; -62.080589
9	22-07-2020 19:36	65	5.3E-04	46.390114; -62.101421
10	21-07-2020 20:15	59	4.8E-04	46.392818; -62.090939
11	24-07-2020 19:29	57	4.6E-04	46.398132; -62.080959
12	22-07-2020 17:04	55	4.4E-04	46.386448; -62.107201
13	24-07-2020 19:30	48	3.9E-04	46.396732; -62.08556
14	22-07-2020 19:37	48	3.9E-04	46.390339; -62.100193
15	24-07-2020 19:36	41	3.3E-04	46.394882; -62.089233
16	24-07-2020 19:31	31	2.5E-04	46.396442; -62.086929
17	24-07-2020 18:13	25	2.0E-04	46.386459; -62.118565
18	21-07-2020 20:15	22	1.8E-04	46.392975; -62.090805
19	24-07-2020 18:18	21	1.6E-04	46.386646; -62.111988
20	24-07-2020 19:36	15.9	1.2E-04	46.394653; -62.088825
21	22-07-2020 19:37	13.3	1.0E-04	46.390591; -62.099422
22	22-07-2020 17:07	12.6	9.7E-05	46.386269; -62.110722
23	21-07-2020 20:16	11.2	8.6E-05	46.393421; -62.089939
24	24-07-2020 19:31	9.2	7.0E-05	46.396744; -62.085999
25	24-07-2020 18:15	7.4	5.6E-05	46.38686; -62.116539
26	24-07-2020 18:14	6.7	5.1E-05	46.386528; -62.118763
27	21-07-2020 20:16	3.1	2.3E-05	46.393661; -62.089458
28	24-07-2020 18:13	2.4	1.7E-05	46.386433; -62.11874
29	21-07-2020 20:16	2.0	1.4E-05	46.393745; -62.089233
30	24-07-2020 19:37	1.9	1.4E-05	46.393871; -62.089138
31	21-07-2020 20:14	1.7	1.2E-05	46.392387; -62.092205

*Measured spring discharges used in the plume size-spring discharge relationship. The accuracy of measured discharges was estimated to be within $\pm 25\%$.

Table S3: Summary of groundwater springs, baseflow-fed streams and shallow porewaters collected in August and November 2020. Porewater values in parentheses indicate sample collection depth. Stream locations are shown in Figure 1.

Sample ID	Sample Type	Temperature (°C)	Salinity (psu)	²²² Rn (Bq m ⁻³)
<i>August 2020</i>				
Spring A	fractured sandstone spring	8.6	0.93	8,360 ± 1,280
Spring B(1)	fractured sandstone spring	9.8	0.76	10,080 ± 1,670
Spring B(2)	fractured sandstone spring	9.4	0.87	16,570 ± 1,180
Spring C	fractured sandstone spring	11.6	0.25	6,740 ± 880
<i>November 2020</i>				
Spring A	fractured sandstone spring	7.9	0.87	7,530 ± 1,060
Spring B(1)	fractured sandstone spring	9.5	0.71	13,220 ± 470
Spring B(2)	fractured sandstone spring	9.2	0.80	12,620 ± 680
Spring C	fractured sandstone spring	9.3	0.21	7,880 ± 770
Stream S1	Stream	5.3	0.25	3,410 ± 590
Stream S2	Stream	5.0	0.30	410 ± 100
Stream S3	Stream	6.2	0.15	360 ± 110
Stream S4	Stream	6.1	0.15	360 ± 60
Stream S6	Stream	6.2	0.13	940 ± 140
WT1	Porewater (0.2 m)	0.7	16.6	710 ± 300
WT2	Porewater (0.4 m)	0.7	17.3	1,000 ± 410
OP1	Porewater (0.2 m)	7.9	19.6	500 ± 240
MP2	Porewater (0.4 m)	1.6	18.0	340 ± 140

Table S4: Summary of parameters and fluxes used in the ²²²Rn mass balance.

Term	Definition	Value	Uncertainty	Units
A	Lagoon area	5.90E+05	5.90E+04	m ²
I	Mean excess ²²² Rn inventory	18	15	Bq m ⁻²
Q _{stream}	Stream discharge	0.05	0.02	m ³ s ⁻¹
C _{stream}	Stream ²²² Rn	1100	1200	Bq m ⁻³
C _{GW}	Fractured-sandstone spring ²²² Rn	10400	3700	Bq m ⁻³
C _{Ra}	²²⁶ Ra activity	10	8	Bq m ⁻³
λ _{Rn}	²²² Rn decay constant	0.181	-	d ⁻¹
<i>²²²Rn Sinks</i>				
J _{atm}	Atmospheric evasion	6.4E+06	6.6E+06	Bq d ⁻¹
J _{mix}	Mixing losses	8.4E+07	5.9E+07	Bq d ⁻¹
J _{decay}	Radioactive decay	1.9E+06	1.6E+06	Bq d ⁻¹
<i>²²²Rn Sources</i>				
J _{diff}	Molecular diffusion	6.4E+06	3.2E+06	Bq d ⁻¹
J _{Ra-226}	²²⁶ Ra production	1.1E+06	8.5E+05	Bq d ⁻¹
J _{stream}	Stream ²²² Rn flux (inc. baseflow)	4.7E+06	5.6E+06	Bq d ⁻¹
J _{spring}	Groundwater ²²² Rn	8.0E+07	6.0E+07	Bq d ⁻¹
-	Groundwater discharge	0.09	0.07	m ³ s ⁻¹

Table S5. Coarse calibration targets based on field data (transducer measuring groundwater temperature in coastal piezometer, see Figure 1, main text) compared with SHAW modelled results covering this sampling period.

Data ID	Depth (m)	Temperature (°C)	Amplitude (°C)	Lag (days)
Coastal piezometer	4.24	5.10 - 9.50 ¹	1.80 – 2.20 ¹	70 – 100
SHAW Simulation	4.20	7.45 – 7.80 ²	2.10 – 2.20 ^{2,3}	92 – 105

¹Range of groundwater temperatures measured from 15-minute resolution temperature data gathered discontinuously over a period of two years (2019-2020) from a coastal piezometer (see Figure 1) adjacent to the Basin Head lagoon.

²Range of average annual temperature output from the SHAW simulation between 2016 to 2020.

³To assess our model output, we also used a provincial monitoring well located nearby the Basin Head watershed that had a sensor at a depth of 13.9 m. Our modeled temperature amplitude at this point was close to the measured amplitude, but off by 0.1°C.

A high-level sensitivity analysis was conducted on model parameters and design elements that were highly uncertain and expected to affect the calibration targets (i.e., subsurface temperature patterns). This assessment focused on the calibration performance and, by extension, the thermal control of the model. The estimated likely range of each of the model parameters/elements listed in Table S6 were tested one at a time. To reflect the high degree of uncertainty involved in this modelling process, only relative qualitative indicators of sensitivity were used for the tested parameters (i.e., low [L], medium [M], and high [H] sensitivity) based on the magnitude of their influence on calibration performance over their expected range (i.e., how much they changed the subsurface temperatures of the domain). Table S6 presents the resultant uncertainty (binned into three categories) for each parameter.

Table S6. Qualitative, relative attribution of sensitivity to SHAW model input parameters. Letters indicate low (L), medium (M), and high (H) model sensitivity to the respective parameter.

Model Parameter/Element	Sensitivity
Residue layer	H
Lower boundary temperature	H
Lower boundary depth	M
Snow/rain threshold	M
Water table depth	M
Shallow organic content	L
Initial domain temperatures	L
Soil compositions	L
Soil porosity	L
Soil density	L

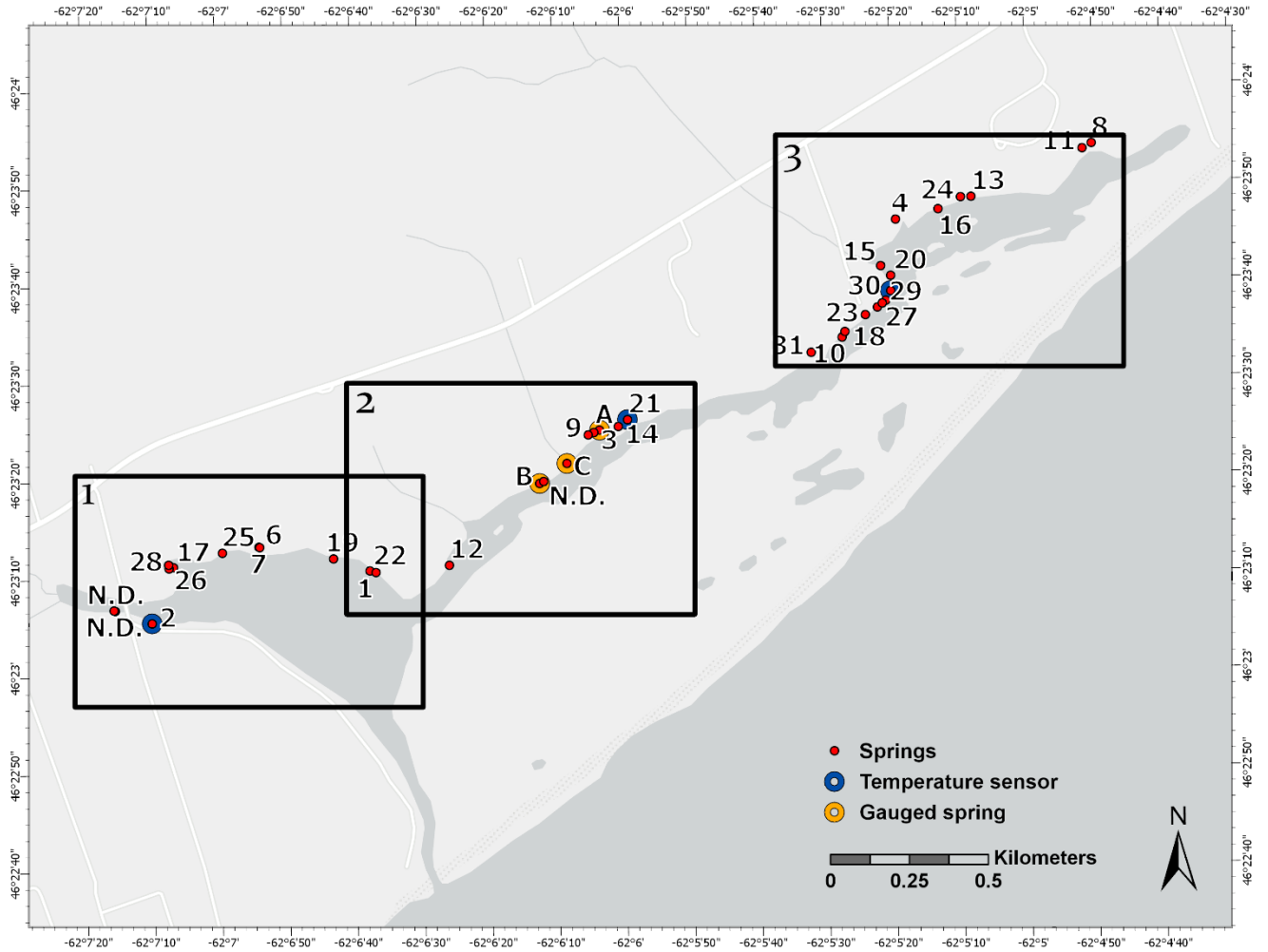


Figure S3. (Series image 1 of 4) Spring locations in the Basin Head lagoon. Black boxes each represent an area depicted in subsequent series images that include spring IDs with reference to Table S1: (1) Figure S4, (2) Figure S5, and (3) Figure S6. Basemap is attributed to Esri, HERE, Garmin, FAO, NOAA, USGS, © OpenStreetMap contributors, and the GIS User Community.

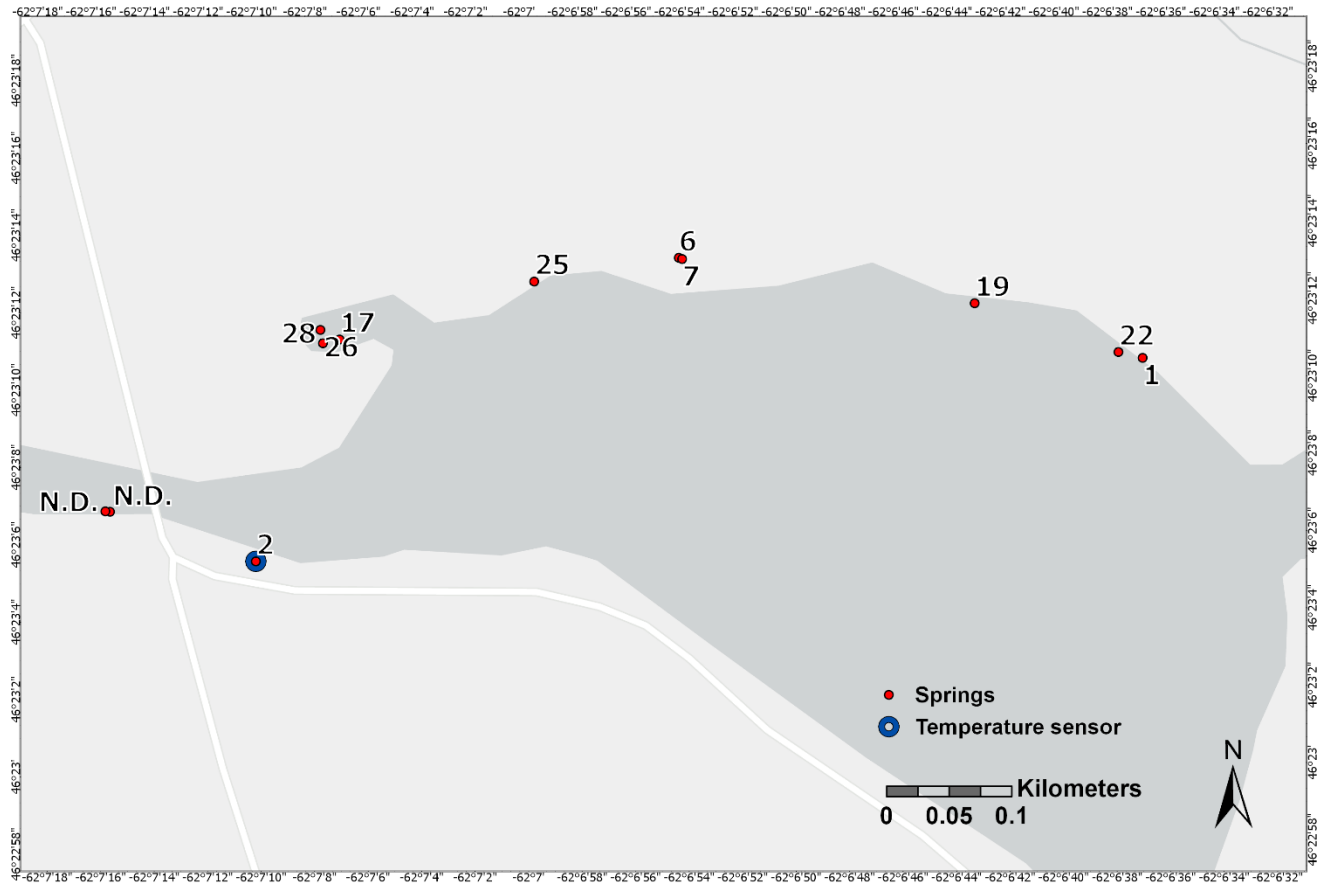


Figure S4. (Series image 2 of 4, see box 1 Fig. S3) Locations and IDs of springs in main basin of the Basin Head lagoon. N.D. = No Data. Basemap is attributed to Esri, HERE, Garmin, FAO, NOAA, USGS, © OpenStreetMap contributors, and the GIS User Community.

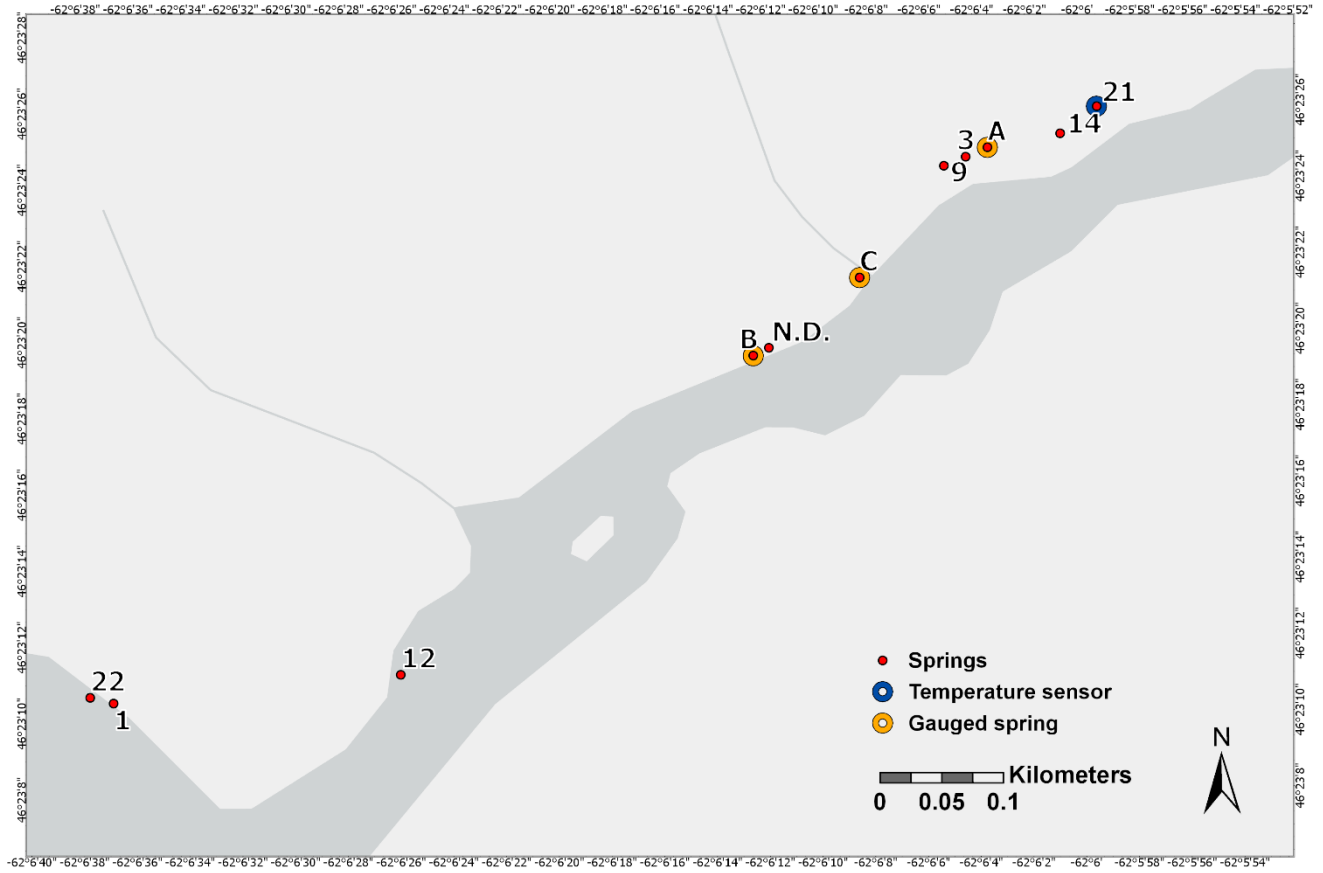


Figure S5. (Series image 3 of 4, see box 2 Fig. S3) Locations and IDs of springs in the main basin and north-east arm of the Basin Head lagoon. N.D. = No Data. Map prepared in ArcGIS Pro (Version 2.3.3, 2018). Basemap is attributed to Esri, HERE, Garmin, FAO, NOAA, USGS, © OpenStreetMap contributors, and the GIS User Community.

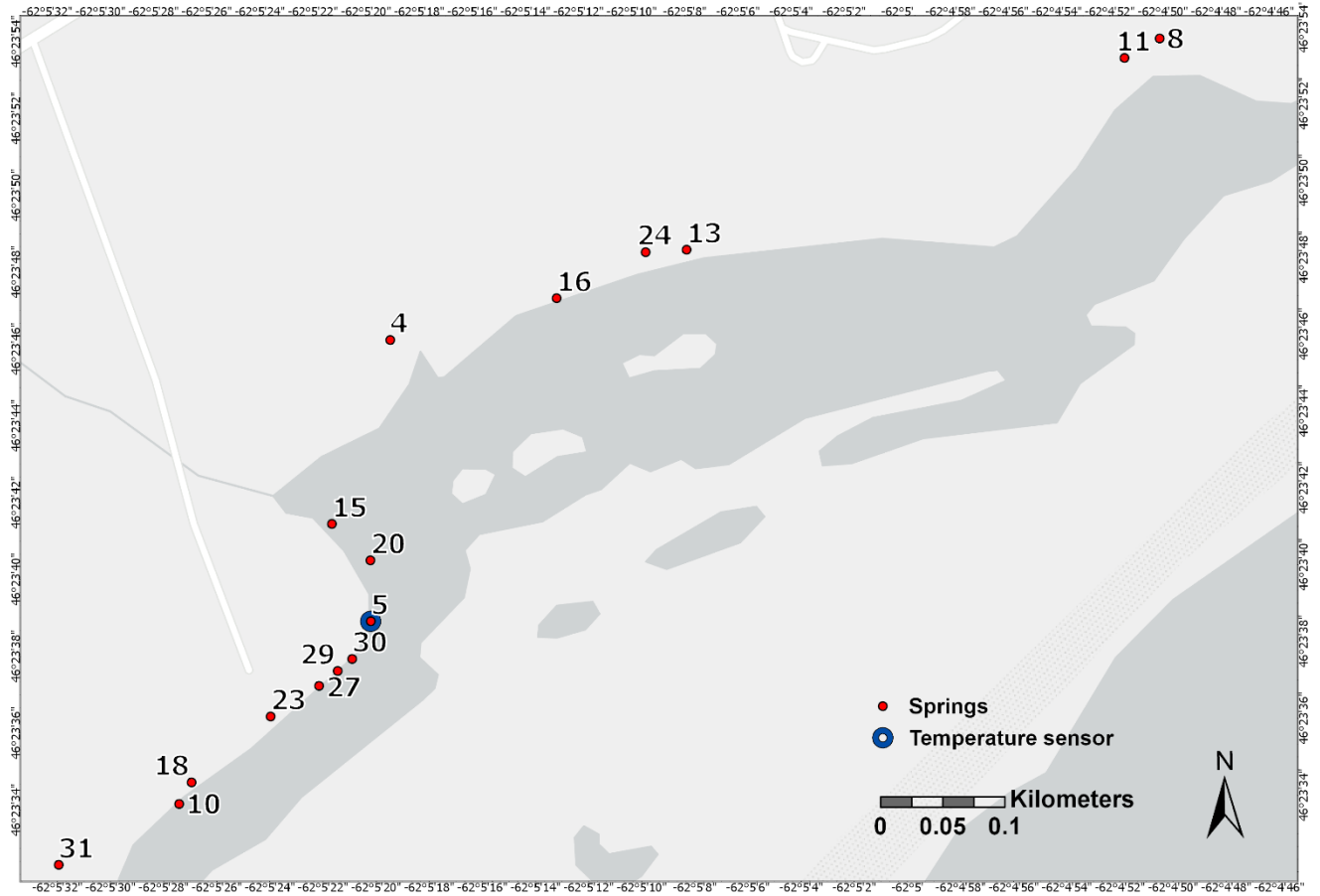


Figure S6. (Series image 4 of 4, see box 3 Fig. S3) Locations and IDs of springs in the upper north-east arm of the Basin Head lagoon. Basemap is attributed to Esri, HERE, Garmin, FAO, NOAA, USGS, © OpenStreetMap contributors, and the GIS User Community.

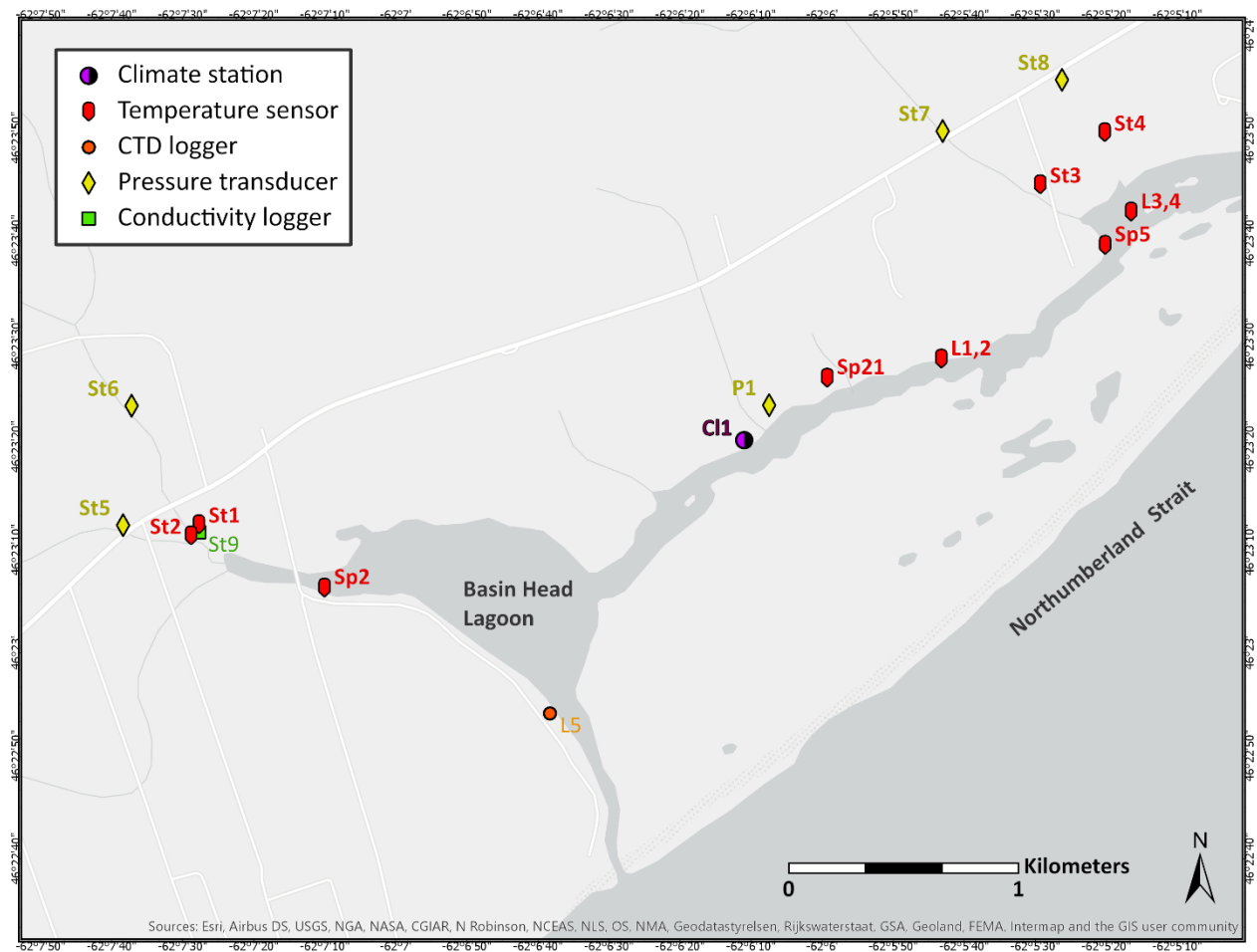


Figure S7: A map of all sensors with data include in the data archive (see Data Availability section of main paper). This additional map is included to provide context for the Sensor IDs noted in Table S1, which correspond to the sensor IDs in the figure. To enable the clear presentation of the sensor IDs, no springs are shown in this figure. Basemap is attributed to Esri, HERE, Garmin, FAO, NOAA, USGS, © OpenStreetMap contributors, and the GIS User Community.

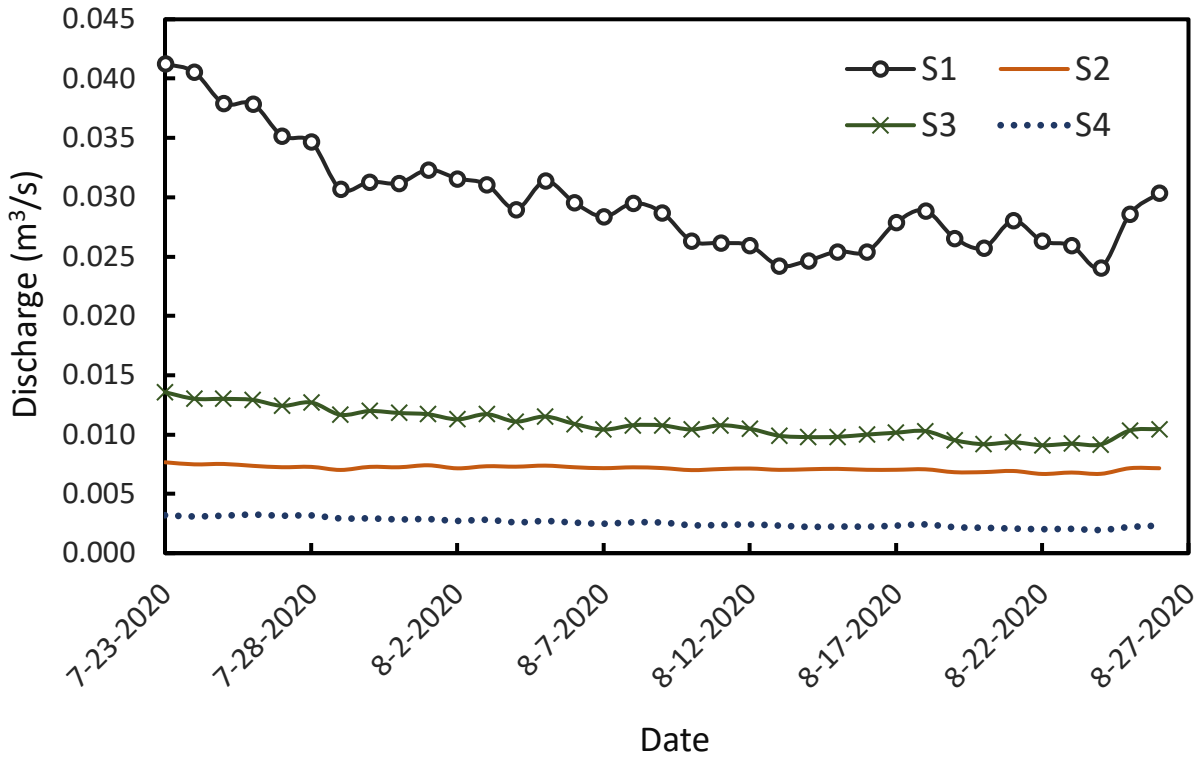


Figure S8: Daily stream hydrographs of the primary four tributaries discharging to Basin Head lagoon over the 35-day focussed study period (date presented as yyyy-mm-dd). Discharge is entirely attributed to baseflow over this period. See Figs. 1 or S7 for locations.

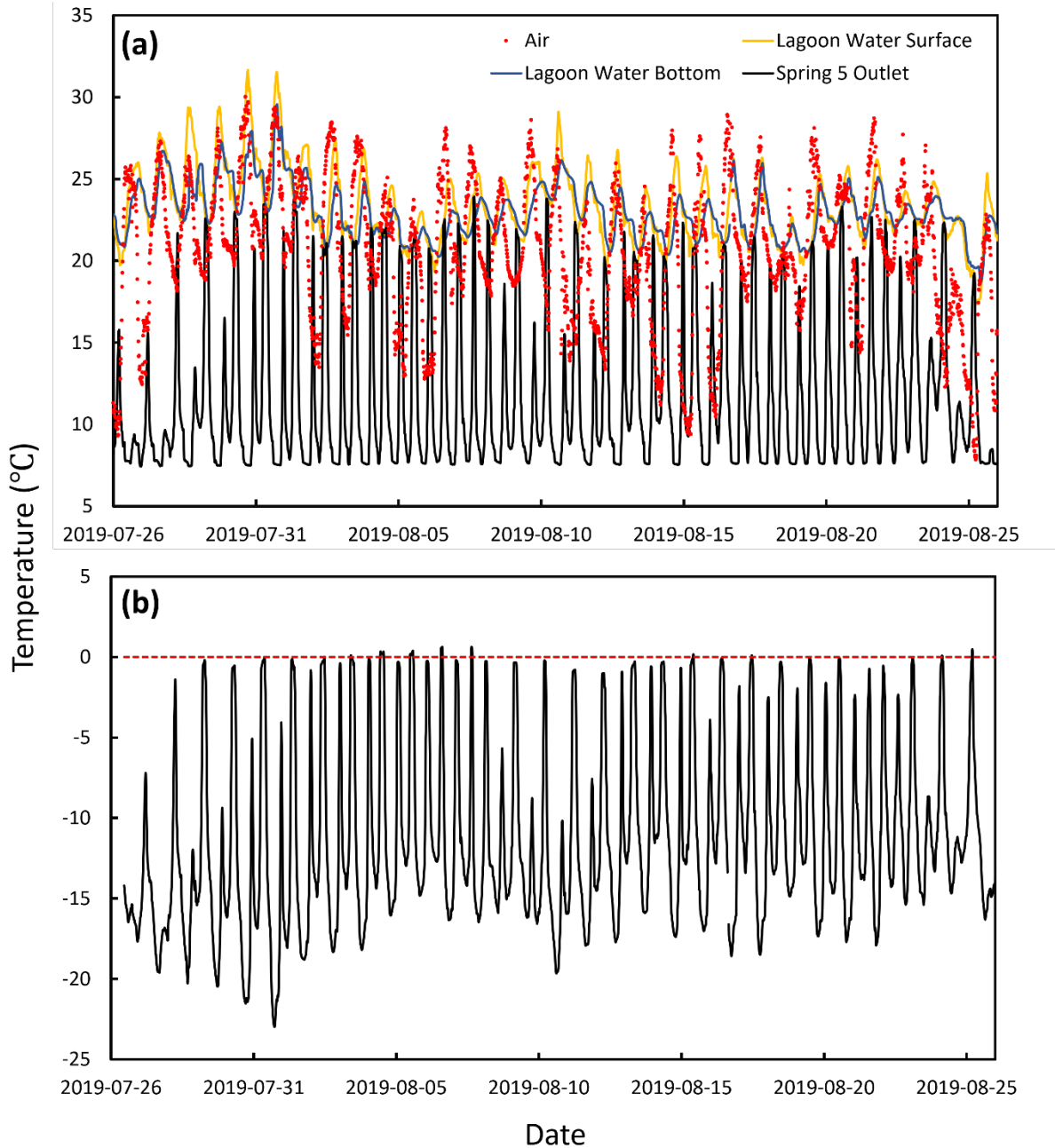


Figure S9: (a) Hourly local air temperature and water temperature data (top and bottom of water column, sensors L3 and L4, respectively, Figure S7) from the upper north-east arm of Basin Head lagoon (date presented as yyyy-mm-dd). (b) The difference between Spring 5 temperature and the average of the channel surface and bottom temperature (shown in a) approximately 30 m away. This difference demonstrates the local cooling effect of springs on the lagoon water temperature and can be inserted into Eq. (1) in the main text.